Determining the hyperfine structure constants of caesium $8S_{1/2}$ state aided by atomic coherence

2014 Meas. Sci. Technol. 25 035501

(http://iopscience.iop.org/0957-0233/25/3/035501)

IOP Publishing Measurement Science and Technology
Meas. Sci. Technol. **25** (2014) 035501 (8pp) doi:10.1088/0957-0233/25/3/035501

Determining the hyperfine structure constants of caesium $8S_{1/2}$ state aided by atomic coherence

Jie Wang, Huifeng Liu, Baodong Yang, Jun He and Junmin Wang[1]

State Key Laboratory of Quantum Optics and Quantum Optics Devices (Shanxi University) and Institute of Opto-Electronics, Shanxi University, No 92 Wu Cheng Road, Tai Yuan 030006, Shan Xi Province, People's Republic of China

E-mail: wwjjmm@sxu.edu.cn (Junmin Wang)

Received 11 November 2013, revised 15 December 2013
Accepted for publication 20 December 2013
Published 11 February 2014

Abstract

High-sensitivity spectroscopy of caesium's higher excited $8S_{1/2}$ state is obtained by a coherent two-photon transition via an intermediate resonance state. The ladder-type atomic system is driven by two counter-propagating low-power diode lasers, the probe laser being tuned to the transition from the ground state to the intermediate state ($6S_{1/2}$–$6P_{1/2}$), and the coupling laser to that between the intermediate and the final state ($6P_{1/2}$–$8S_{1/2}$). By locking the probe laser and scanning the coupling laser, the electromagnetically induced transparency (EIT) peaks appear in the probe transmission when the coupling laser resonates with each of the hyperfine levels. Compared with conventional EIT, where the signal-to-noise ratio is limited by the absorptive Doppler background, here these narrow-linewidth peaks have no Doppler background. The peak centres are well determined from theoretical fits to the experimental data. To accurately measure the $8S_{1/2}$ hyperfine structure splitting, we developed a simple method to eliminate error arising from the nonlinear frequency scanning by employing an optical waveguide phase modulator and a confocal Fabry–Perot cavity. The hyperfine structure constants of the caesium $8S_{1/2}$ state are obtained from hyperfine structure splitting measurements. Systematic effects from the ac-Stark and Zeeman shifts are studied. The measured hyperfine magnetic dipole constant $A = (219.08 \pm 0.12)$ MHz is consistent with previous results.

Keywords: hyperfine structure constant, caesium $8S_{1/2}$ state, electromagnetically induced transparency, optical waveguide phase modulator

(Some figures may appear in colour only in the online journal)

1. Introduction

Measurements of the hyperfine structure in atomic excited states are important because the states are used in diverse experiments ranging from atomic signatures of parity non-conservation [1] to resonance ionization mass spectrometry [2]. The hyperfine structure splittings (HFSs) of excited states, where electron correlations are less complicated, are more sensitive to nuclear structure details. Knowledge of the hyperfine structure thus provides valuable information about the structure of the nucleus (nuclear deformation) and its influence on the atomic wavefunctions.

Hyperfine spectroscopy of atomic excited states, such as the 8S or 7D states of caesium (Cs), is complicated by the fact that the electric dipole transitions to the ground state are forbidden and must be accessed through weak equal-frequency two-photon transitions [3, 4]. In contrast, a two-step excitation using lower power lasers via an intermediate state in the ladder-type atomic system produces a strong interaction. Employing the optical–optical double-resonance technique [5, 6], researchers can easily obtain excitation spectra, but sometimes the spectra have low signal-to-noise ratios (SNR)

[1] Author to whom any correspondence should be addressed.

because an intermediate state with a large spontaneous emission rate is not easily populated. An alternative method, called the double-resonance optical pumping method, is to detect the variation of the ground-state population instead of the intermediate-state population [7–10]. This is performed by velocity-selective optical pumping from one of the ground-state hyperfine components to another via the two-photon excitation process and spontaneous decay. However, for some close transitions, this two-photon optical pumping effect is too weak to produce observable spectrum amplitude. Electromagnetically induced transparency (EIT) techniques have several practical applications in probe amplification [11], lasing without inversion [12] and suppression of spontaneous emissions [13]. The ladder-type EIT can be used to study the (hyper-)fine structure of high Rydberg states via an intermediate state. Importantly, the method of detecting the transmission of the probe field in EIT while scanning the frequency of the coupling laser can overcome the low oscillator strengths of high nS or nD states [14–16]. In related studies, the feasibility of high-resolution spectroscopy, which uses EIT in a Doppler-broadened medium, is also examined by integrating over all velocity groups. The extent to which different velocity groups affect the EIT signal is nearly neutralized by the counter-propagation of the probe and coupling fields. Consequently, the narrower linewidth allows one to evaluate peak position better [17, 18].

In frequency measurements, the optical-frequency comb provides perfect accuracy [19, 20], but it is too complicated and expensive to use. Fortunately, we are usually concerned with relative frequencies or frequency intervals between hyperfine components. This can be easily performed by optical techniques using an acousto-optic modulator [21], electro-optic modulator (EOM) [22], or a frequency analyser as a Fabry–Perot (F–P) cavity [23]. However, the error arising from a nonlinear frequency scan is difficult to remove while calibrating the frequency axis. In this paper, we achieve high-resolution spectroscopy of the hyperfine structure in excited states using ladder-type EIT. By detecting the transmission of the frequency-fixed probe laser while scanning the frequency of the coupling laser, the EIT spectra are without a Doppler background, as can also be seen in our earlier works in [8, 24, 25]. The frequency interval calibration is performed using the transmitted peaks through the F–P cavity in which the coupling laser is phase-modulated using an EOM. By selecting an appropriate radio frequency that drives the EOM and an appropriate length of cavity, the F–P peaks appear simultaneously with the EIT peaks. Hence, the error arising from nonlinear frequency scanning is eliminated. The systematic effects from the ac-Stark and Zeeman shifts on measurements of the HFS are also studied.

2. Principle and experimental setup

2.1. Principle

Figure 1 shows the energy levels associated with the ladder-type EIT. Traditionally, i.e. in [26], the EIT signal is observed by scanning the frequency of the probe laser, while locking the frequency of the coupling laser. The drawback of this approach is that the EIT signal arises from the centre of the Doppler absorptive profile, and thus the SNR is still limited by the absorptive background. However, the signal in our experimental scheme, obtained by fixing the probe laser frequency while scanning the coupling laser frequency, is background-free. The background-free EIT signal elicits the benefit of a precise determination of the centre frequency of the EIT resonance peaks. In the weak probe region, the linewidth of the signal can be narrowed to a few megahertz and is of great potential for the field of atomic spectroscopy. The frequency of the probe laser ω_p is set to the hyperfine transition Cs $6S_{1/2}(F = 3$ or $4)$–$6P_{1/2}(F' = 3$ or $4)$ at 894.6 nm. Then the frequency of the coupling laser, ω_c, is scanned over the transition Cs $6P_{1/2}(F' = 3$ or $4)$–$8S_{1/2}(F'' = 3$ and $4)$ at 761.1 nm. The decay rates of the intermediate state $6P_{1/2}$ and the excited state $8S_{1/2}$ are denoted by Γ_2 and Γ_3, which are 4.57 MHz and 2.18 MHz, respectively.

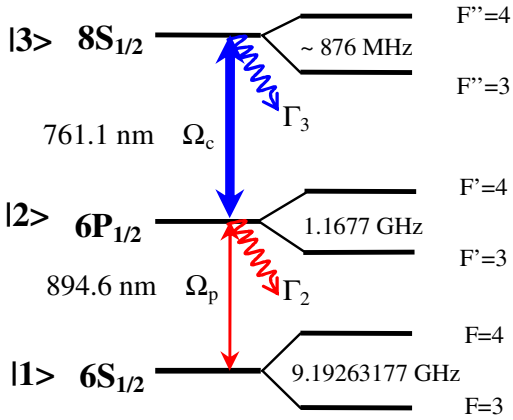

Figure 1. Relevant hyperfine levels of caesium. The intense coupling laser with Rabi frequency Ω_c drives the $|2\rangle$–$|3\rangle$ transition, while the weak probe laser with Rabi frequency Ω_p drives the $|1\rangle$–$|2\rangle$ transition ($\Omega_p < \Gamma_2$).

In room-temperature atomic vapour with number density N_0, the distribution of atomic velocity has a very wide range, and the Doppler effect should be taken into account. The number density with velocity v is $N(v)\mathrm{d}v = \frac{N_0}{u\sqrt{\pi}}\mathrm{e}^{v^2/u^2}\mathrm{d}v$, where $u = \sqrt{\frac{2kT}{m}}$ is the most probable speed. Their contribution to the total susceptibility χ can be derived from standard semi-classical methods [26]:

$$\chi(v)\,\mathrm{d}v = \frac{4\mathrm{i}\hbar g_{21}^2/\varepsilon_0}{\gamma_{21} - \mathrm{i}\Delta_p - \mathrm{i}\frac{\omega_p}{c}v + \frac{\Omega_c^2/4}{\gamma_{31} - \mathrm{i}(\Delta_p+\Delta_c) - \mathrm{i}(\vec{k}_p+\vec{k}_c)\cdot\vec{v}}} \times N(v)\,\mathrm{d}v. \quad (1)$$

Here, the detunings $\Delta_p = \omega_p - \omega_{12}$ and $\Delta_c = \omega_c - \omega_{32}$ are defined as the nominal detunings for an atom at rest, and $2\hbar g_{21}$ is the dipole moment matrix element. If collisional dephasing is negligible, the decay rates are given by $\gamma_{ij} = (\Gamma_i + \Gamma_j)/2$, where Γ_i is the natural decay rate of level $|i\rangle$ (with $\Gamma_1 = 0$, since level $|1\rangle$ is the ground state). Considering the laser linewidths of γ_p for the probe laser and γ_c for the coupling laser, we change the effective linewidths [26] $\gamma_{21} \to \gamma_{21} + \gamma_p$, $\gamma_{31} \to \gamma_{31} + \gamma_p + \gamma_c$. Because of the Doppler-broadened velocity distribution,

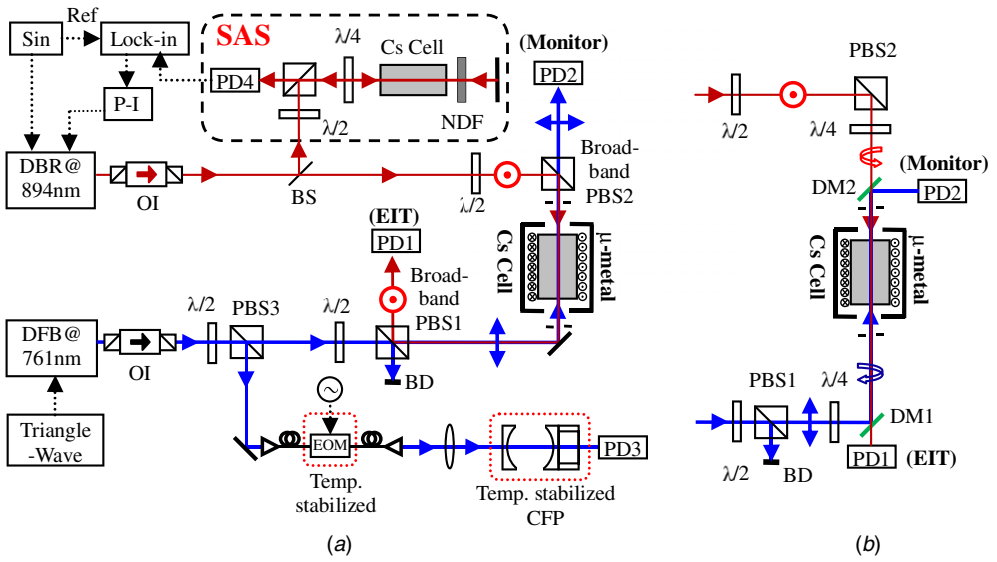

Figure 2. Schematic diagram of the experiment. (*a*) The two lasers are perpendicularly-linear polarized in front of the cell. (*b*) The two lasers are circularly polarized in front of the cell. Keys to figure: SIN: sine-wave signal generator; Ref: reference channel of lock-in amplifier; Lock-in: lock-in amplifier; PD: photodiode; SAS: saturated absorption spectroscopy; P–I: proportion and integration amplifier; $\lambda/2$: half-wave plate; $\lambda/4$: quarter-wave plate; NDF: natural density filter; OI: optical isolator; PBS: polarization beam splitter cube; BS, beam splitter; BD, beam dump; μ-metal, magnetic metal; EOM, electro-optic modulator; CFP: confocal F–P cavity; DM: 45° dichroic mirror.

the term $\mathrm{i}(\vec{k}_\mathrm{p}+\vec{k}_\mathrm{c})\cdot\vec{v}$ does make a difference. Its value is smallest, $\mathrm{i}(\omega_\mathrm{p}-\omega_\mathrm{c})\cdot v/c$, for the counter-propagating (CTP) configuration, and becomes largest, $\mathrm{i}(\omega_\mathrm{p}+\omega_\mathrm{c})\cdot v/c$, for the co-propagating (CP) configuration. With a weak probe field, the population in levels $|2\rangle$ and $|3\rangle$ is almost negligible. Hence, the two kinds of optical pumping effects, single-resonance optical pumping and double-resonance optical pumping, need not be considered.

By numerically integrating over all velocity groups, we can obtain the total susceptibility$\chi=\chi'+\mathrm{i}\chi''$; the real part χ' and the imaginary part χ'' are related to the dispersion and absorption of the atomic medium. Based on the imaginary part, we fitted the EIT peaks to determine their intervals. Additionally, the extent to which different velocity groups affect the EIT signal is nearly neutralized by the counter-propagation of the probe and coupling fields. Consequently, the narrowing linewidth allows one to evaluate peak positions better. Furthermore, in a weak probe field regime and when integrating over the velocity groups, absorption is enhanced on both sides of the EIT signal [17].

The hyperfine structure results from the coupling of the total electron angular momentum **J** with the total nuclear angular momentum **I**. The nucleus has a magnetic dipole moment and an electric quadrupole moment, which are related to the spin angular momentum and the aspherical spatial charge distribution, respectively. The interaction of the nuclear magnetic dipole moment with the magnetic flux density created by atomic electrons and the interaction of the electric quadrupole moment with the gradient of the electric field at the nucleus give rise to the hyperfine structure interaction [27, 28]. The total hyperfine energy shift is

$$\Delta E_\mathrm{hfs}=\frac{1}{2}A_\mathrm{hfs}K+\frac{B_\mathrm{hfs}}{4}\frac{\frac{3}{2}K(K+1)-2I(I+1)J(J+1)}{I(2I-1)J(2J-1)}, \quad (2)$$

where $K=F(F+1)-I(I+1)-J(J+1)$, I is the nuclear spin angular momentum quantum number, J the total electron angular momentum quantum number, F the total angular momentum quantum number, A_hfs the magnetic dipole constant and B_hfs the electric quadrupole constant. For a given state with I and J, the HFS from F to $F-1$ is derived as

$$\begin{aligned}\Delta E_\mathrm{hfs}(F\to F-1)&=\Delta E_\mathrm{hfs}(F)-\Delta E_\mathrm{hfs}(F-1)\\&=A_\mathrm{hfs}F+B_\mathrm{hfs}\frac{\frac{3}{2}F\left[F^2-I(I+1)-J(J+1)+\frac{1}{2}\right]}{I(2I-1)J(2J-1)}.\end{aligned} \quad (3)$$

For the caesium $8S_{1/2}$ state, the gradient of the electric field at the nucleus is zero for a spherical electron wavefunction; hence, there is no electric quadrupole hyperfine interaction, thus $B_\mathrm{hfs}=0$. Therefore, the relationship between the HFS and the magnetic dipole constant in this state reads

$$\Delta E_\mathrm{hfs}(8S_{1/2},\quad F''=4\to F''=3)=A_\mathrm{hfs}\times 4. \quad (4)$$

The magnetic dipole constant of $8S_{1/2}$ is determined in the easiest way by measuring the HFS.

2.2. Experimental setup

A schematic diagram of the experimental setup is given in figure 2(*a*). A distributed-feedback (DFB) diode laser operating at 761.1 nm with a typical linewidth of ~1 MHz serves as the coupling laser scanning over the $6P_{1/2}$–$8S_{1/2}$ transition, while a distributed-Bragg-reflector (DBR) diode laser operating at 894.6 nm with a typical linewidth of ~1 MHz is used as the probe laser. The latter can be locked to one of the $6S_{1/2}$–$6P_{1/2}$ hyperfine transitions using the conventional frequency modulation technique combined with saturated absorption spectroscopy. In our experiment, the coupling and probe lasers are in the CTP configuration to

partly eliminate the Doppler effect when $\omega_p \sim \omega_c$. The two unfocused laser beams have a Gaussian waist ($1/e^2$ intensity radius) of 0.54 mm for the probe beam and 0.66 mm for the coupling beam. They overlap in the caesium vapour cell (25 mm in diameter, 75 mm in length and with magnetic shield) with broad-band polarization beam splitters (PBSs). The probe beam is then separated by PBS1 and directed to photodiode 1 (PD1). The EIT spectra without the Doppler background from PD1 are recorded by a digital storage oscilloscope (not shown in figure 2). A part of the coupling laser separated from PBS3 couples to a fibre-pigtailed waveguide-type phase EOM driven by a known radio frequency, then passed through a confocal F–P cavity (with a finesse of 120 and a free spectral range of 2.5 GHz) and directed to PD3. The F–P signal, including one carrier and two sidebands from PD3, is recorded to calibrate the hyperfine frequency interval. The solenoid coil around the cell, which is placed inside the magnetic shielding tank, is used to examine systematic effects arising from the longitudinal magnetic field. For comparison, we studied these effects when the two beams are circularly polarized by inserting corresponding quarter-wave plates and two 45° dichroic mirrors, as in figure 2(*b*). Considering the weak probe field for EIT [26], the power of the probe laser is set as 1.14 μW and the intensity is 0.12 mW cm^{-2}. The power of the coupling laser is set to 10.0 mW and the intensity at 730 mW cm^{-2}.

To eliminate error arising from the nonlinear frequency scanning of the coupling laser, we developed a simple frequency calibration method employing an optical waveguide phase modulator and a confocal F–P cavity. First, by scanning the coupling laser's frequency, we obtained the EIT spectra and F–P signal from PD1 and PD3, respectively, and simultaneously recorded the data on a digital storage oscilloscope. Second, we moved one of the F–P peaks to the middle of the two EIT peaks by adjusting the length of the F–P cavity via the voltage driving the piezoelectric actuator. We used a radio frequency to drive the EOM, setting the frequency very close to half the EIT peak interval. Thus, the sideband peaks and EIT peaks appear simultaneously and the nonlinear error in frequency is eliminated. Here, the radio frequency is 440.000 MHz and the frequency interval of the two sidebands is 880.000 MHz, which is near the HFS (∼876 MHz) for the Cs $8S_{1/2}$ state.

To reduce systematic error from the calibrator combining the EOM with the F–P cavity, we take some appropriate measurements. (1) The DFB laser is chosen as the coupling laser for better mechanical stability compared with the external cavity diode laser. (2) The F–P cavity is temperature-controlled at 25 °C against temperature changes that can vary the cavity length and cause the centre of the signal to move. (3) Similarly, the temperature of the large-bandwidth (∼10 GHz) EOM modulated by a PSG analogue signal generator (Agilent, E8257D) is controlled at 18 °C by a unit comprising five thermoelectric coolers.

3. Experimental results

In the Cs $6S_{1/2}$–$6P_{1/2}$–$8S_{1/2}$ ladder-type system, the weak probe laser is locked to the lower transition, whereas the strong coupling laser is scanned across the upper transition. The EIT peaks appear in the probe transmission when the coupling laser is in resonance with a hyperfine level. In this arrangement, the centres of the EIT peaks are well determined by fitting the curves, for they have no Doppler background compared with conventional EIT signals. Figure 3 shows the typical experimental data of an EIT spectrum with scanning coupling frequency for the hyperfine transition channel $6S_{1/2}(F=4)$–$6P_{1/2}(F'=4)$–$8S_{1/2}(F''=3)$. The linewidth of the EIT peak is about 8 MHz. We fitted the experimental data with theoretical formula (1) for the ladder-type EIT by numerically integrating over velocity groups ranging from −450 to 450 m s^{-1} in unit steps of 1 m s^{-1} (99.9% of atoms are contained in the Maxwell velocity distribution); the fitting residual suggests an excellent fit. The horizontal coordinate is calibrated by the following method.

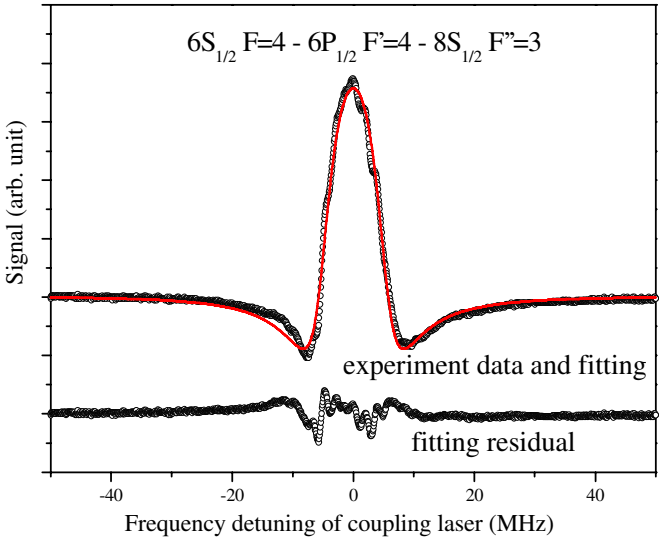

Figure 3. Typical experimental data and fit of an EIT spectrum with scanning coupling frequency corresponding to the hyperfine transition channel $6S_{1/2}(F=4)$–$6P_{1/2}(F'=4)$–$8S_{1/2}(F''=3)$. Open circles denote the experimental data and the solid curve represents the fitted result. The lower curve is the fitting residual, which indicates an excellent fit.

By scanning the coupling laser's frequency, we recorded the EIT signal and the transmitted signal of the confocal F–P cavity from PD1 and PD3 using a digital storage oscilloscope. The typical measurements of the HFS through the hyperfine transition channel $6S_{1/2}(F=4)$–$6P_{1/2}(F'=3)$–$8S_{1/2}(F''=3, 4)$ are shown in figure 4. The horizontal coordinates are calibrated using the 880.000 MHz frequency interval of the two modulation sidebands, which is close to the HFS (∼876 MHz) for the Cs $8S_{1/2}$ state. The F–P signal is fitted by a multi-peak Lorentz function. The frequency interval of the two EIT peaks is determined by fitting both to the theoretical formula of the ladder-type EIT. The HFS of the Cs $8S_{1/2}$ state is labelled as $\Delta_{hfs} = \nu \pm \Delta\nu$, where $\Delta\nu$ refers to the fitting error (within 95% confidence interval) which combines the F–P signal fitting error with the EIT signal fitting error. The fitting errors for all our fitting data range between 30 and 60 kHz, with mean 44 kHz. For each of the hyperfine transition channels, $6S_{1/2}(F=3, 4)$–$6P_{1/2}(F'=3, 4)$–$8S_{1/2}(F''=3, 4)$, we recorded

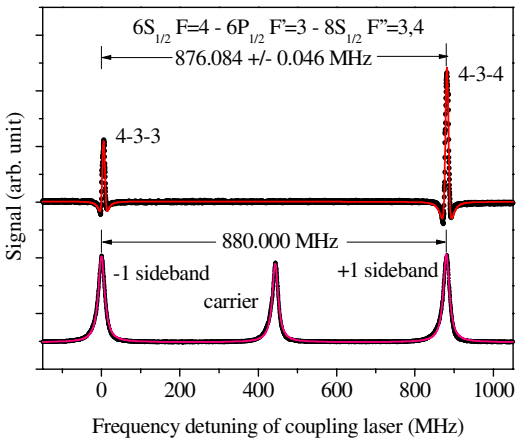

Figure 4. Measurement of the hyperfine structure splitting (HFS) of the Cs $8S_{1/2}$ state through the hyperfine transition channel $6S_{1/2}(F = 4)$–$6P_{1/2}(F' = 3)$–$8S_{1/2}(F'' = 3, 4)$. The lower curve is the transmission signal of the F–P cavity for the scanning coupling laser set at 761.1 nm after the fibre-pigtailed waveguide-type phase modulator. The frequency interval between the +1-order sideband and the −1-order sideband is 880.000 MHz, which is determined by the EOM's driving RF frequency (stabilized by a rubidium clock). The upper curve is the EIT signal. The Cs $6S_{1/2}(F = 4)$–$6P_{1/2}(F' = 3)$–$8S_{1/2}(F'' = 3)$ transition is labelled 4–3–3 and the Cs $6S_{1/2}(F = 4)$–$6P_{1/2}(F' = 3)$–$8S_{1/2}(F'' = 4)$ transition is labelled 4–3–4. The linewidth of the EIT resonance peak is ∼8 MHz. The solid circles denote the experimental data and the solid line represents the fitted result. Both fitting curves show perfect agreement with experimental data. In this way, the HFS between the $F'' = 3$ and $F'' = 4$ levels in the Cs $8S_{1/2}$ state can be measured with very small fitting statistical error.

Table 1. Results of the mean value and standard error for each group of 60 recorded data.

Hyperfine transition channels $6S_{1/2}(F)$–$6P_{1/2}(F')$–$8S_{1/2}(F'')$	Mean (MHz)	Standard error (MHz)
4–3–3, 4 (60 times)	876.257	0.095
4–4–3, 4 (60 times)	876.231	0.111
3–3–3, 4 (60 times)	876.769	0.104
3–4–3, 4 (60 times)	876.029	0.103
The four transition channels	876.322	0.052

the signals 60 times and fitted them to obtain the mean and standard error of the mean (see table 1 for a listing). The differences between these mean values are probably caused by systematic errors. The four results should be consistent with each other and the average gives (876.322 ± 0.052) MHz, where 0.052 MHz refers to statistical error.

4. Systematic effects

An accurate determination of the HFS requires careful attention to a number of possible systematic uncertainties, such as ac-Stark shifts, Zeeman shifts, pressure shifts, error arising from misalignment of the CTP laser beams, the locking offset of the probe laser and uncertainty arising from the frequency interval calibration. The associated uncertainties are summarized in table 2 and described as follows.

Table 2. Error budget for the hyperfine structure splitting measurement (units: kHz).

Systematic effects	Error
Ac-Stark shifts	<492
Zeeman shifts	<0.01
Pressure shifts	<10
Frequency interval calibration	<30
Fitting error	44
Total systematic	495
Statistic error	52
Total	498

4.1. ac-Stark shifts

The effect of ac-Stark shifts on the HFS is investigated by varying the optical powers. Because the probe laser has a very low power of 1.14 μW, we varied the power of the coupling laser from 0.50 to 10.0 mW. Consequently, we obtained a HFS that depended on the coupling laser power, as in figure 5(*a*). We find the slope to be 423(69) kHz/I' ($I' = 730$ mW cm^{-2}), or 0.58(9) kHz/(mW cm^{-2}). Combining the value of the slope with its uncertainty, we arrive at a maximum possible shift of 492 kHz at the operating intensity, $I' = 730$ mW cm^{-2}. We take this value as an estimate of the systematic uncertainty from the ac-Stark effect.

4.2. Zeeman shifts

Strictly speaking, when the lasers propagate parallel to the magnetic field in a Cs vapour cell, π-transitions do not occur [27]. Each of the linearly polarized laser beams in figure 2(*a*) should be considered as the superposition of σ^+ and σ^- components of equal amplitudes. Although the power resonant with the 6S–6P transition is ∼2% of the saturation, there exists some optical pumping that can couple with the external magnetic field. Because of the optical pumping between the Zeeman sublevels, the populations of ground-state atoms are symmetrical distributed over the Zeeman sublevels. Consequently, the magnetic field only broadens but does not shift the peaks via the linear Zeeman shift. However, the laser polarization is not perfectly linear; thus, the amplitudes of the two components are different, which leads to an asymmetric effect. To investigate the effect of the Zeeman shifts from the imperfect magnetic shield, the HFS is measured in a magnetic field generated by the solenoid coil, as shown in figure 2(*a*). Figure 5(*b*) shows the HFS versus magnetic flux density. We find the slope to be 44(29) kHz G^{-1}. In addition, we carefully investigated the dependence of HFS for different polarization combinations of probe and coupling beams on the magnetic flux density. If the two beams have the same circular polarization, as shown in figure 2(*b*), we obtain a maximum slope of 970(27) kHz G^{-1}. That is, the systematic uncertainty from the Zeeman shift for imperfect linear polarization is approximately two orders of magnitude less than that for circular polarization. The reduced magnetic field along the axis of the Cs vapour cell inside the magnetic shielding tank is measured to be less than 0.2 mG, which is $\sim 10^{-3}$ less than the Earth's magnetic field (∼500 mG). We estimated that the maximum possible uncertainty from the Zeeman shift is less

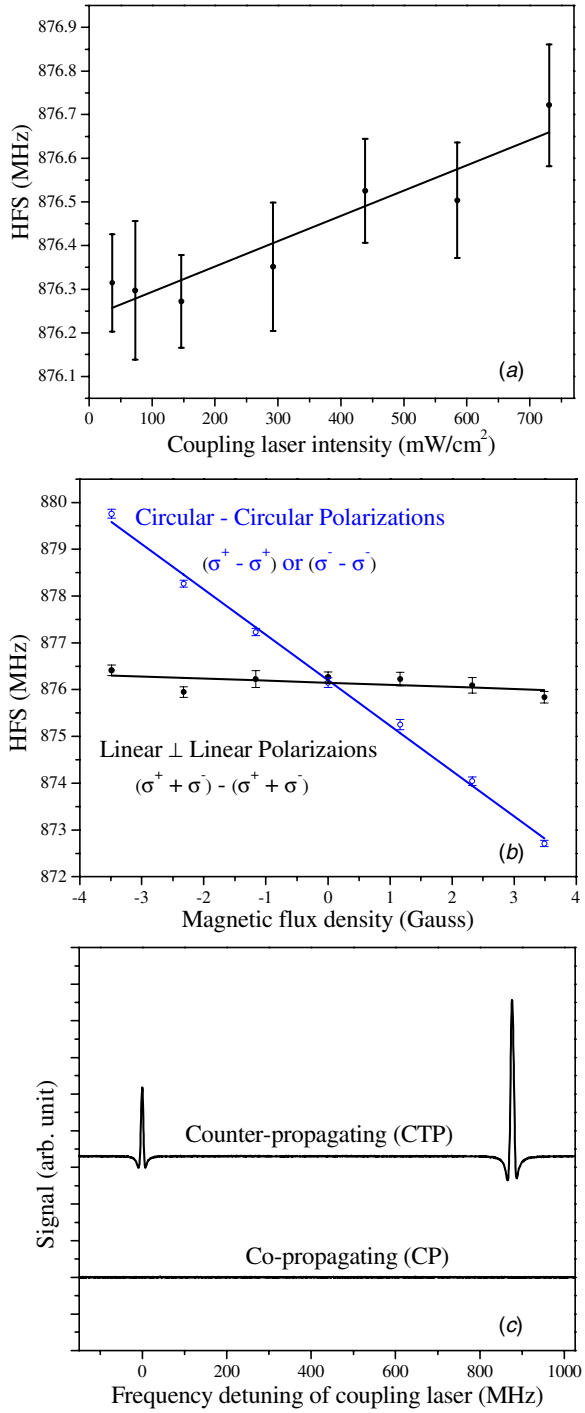

Figure 5. Analysis of systematic effects. (*a*) HFS increases as a function of the coupling laser power due to ac-Stark shift and linear fit—only statistical errors are included in the error bars. (*b*) Zeeman plot of the HFS with both lasers perpendicularly linearly polarized (linear-per-linear, corresponding to $(\sigma^+ + \sigma^-)$–$(\sigma^+ + \sigma^-)$, not π–π) and identically circularly polarized (circular–circular, corresponding to σ^+–σ^+ or σ^-–σ^-) and their linear fit—only statistical errors are included in the error bars. The systematic uncertainty can be reduced by choosing linearly polarized beams as they are insensitive to magnetic fields. (*c*) Detection of the probe laser signals for the coupling laser (10.0 mW) counter-propagating (CTP) and co-propagating (CP) with the probe beam (1.14 μW). There is no signal for the CP case. Consequently, possible systematic effects caused by beam reflection at the cell wall should be cancelled.

than 0.01 kHz, which is negligible compared with the other uncertainties.

4.3. Pressure shifts

To estimate the effect of pressure shifts, we monitored the temperature on the surface of the Cs vapour cell to be ~23 °C, corresponding to a pressure of 1.2×10^{-6} Torr. Theoretically, the pressure shift is the same for the two hyperfine components ($8S_{1/2}(F'' = 3, 4)$). However, based on the previously measured shift of the 6S–8S two-photon transitions, −12(10) kHz mTorr^{-1} for $F = 3$–$F'' = 3$ and −26(10) kHz mTorr^{-1} for $F = 4$–$F'' = 4$ given in [4], and −63.3 kHz mTorr^{-1} given in [19], we expected a shift of less than 0.1 kHz. It is also possible that impurities inside the vapour cell shifted the transition frequency. The uncertainty from impurities is difficult to estimate, but based on Rb and I_2 vapour cell measurements, it is probably not larger than 10 kHz.

4.4. Error arising from the misalignment of the CTP laser beams

Misalignment of the two beams broadens and shifts the peaks through first-order Doppler shift. As can be seen from equation (1), the position of the peaks depends on the difference in the magnitude and direction of the two vectors $\vec{k}_p$ and $\vec{k}_c$. Additionally, first-order Doppler shifts come into play if the wavefronts of $\vec{k}_p$ and $\vec{k}_c$ are not precisely CTP, which can result from a divergence of the CTP beams and a mismatch of the spatial modes. A small angle (less than 2 mrad in our experiment) between the CTP beams should cause the peaks to shift slightly. Note that the atomic velocity distribution is isotropic, the two peaks shift in the same direction equally and their distance remains unchanged. The misalignment however can cause distortions of the line shape, i.e. asymmetries, if a small component of the coupling laser is reflected at the cell wall and interacts with the atoms. To analyse this effect, we made the coupling laser of CP with the probe laser, but see no peaks, as in figure 5(*c*). Hence, the reflected coupling laser has no effect. This correlates with the theoretical analysis given in [26].

4.5. The locking offset of the probe laser

The locking offset of the probe laser can cause detuning of the resonance transition, $\Delta_p \neq 0$, but the systematic line shift is negligible because relative intervals are used. Jitter of the laser frequency causes a difference, but as jitter is random, it can be eliminated by more measurements.

4.6. Uncertainty arising from the frequency interval calibration

The final systematic error considered is the possible error from the instability in the frequency interval calibration. This calibration is performed using the transmitted peaks through the F–P cavity in which the coupling laser is phase-modulated using an EOM. As mentioned before, it depends on the nonlinearity in frequency scanning, the thermal fluctuation and mechanical vibration of the F–P cavity, and the uncertainty in

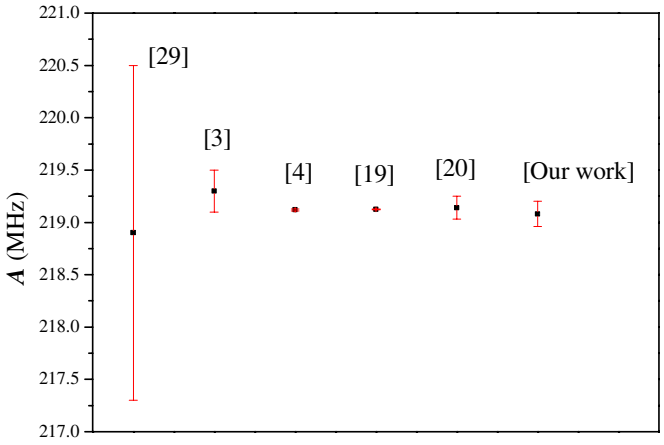

Figure 6. Comparison of experimental results for the hyperfine magnetic dipole constant A of the Cs $8S_{1/2}$ state.

the radio frequency driving the EOM. Given an appropriate length of cavity and an appropriate radio frequency, the F–P peaks appear simultaneously with the EIT peaks. Hence, errors arising from nonlinear frequency scanning cancel. However, a slight difference between the frequency interval of the two sidebands (880.000 MHz) and the HFS (∼876 MHz) for the Cs $8S_{1/2}$ state does cause an error of 30 kHz at the measured nonlinearity of <0.5%. The instability arising from thermal fluctuations and mechanical vibrations of the F–P cavity can be eliminated by making repeated measurements. The accuracy of our PSG analogue signal generator (Agilent E8257D, Palo Alto, CA, USA) is 10^{-6}, causing error in the frequency interval calibration of <1 kHz. According to these analyses, a conservative estimate of the instability of frequency interval calibration is about 30 kHz mainly due to the slight difference between the frequency interval of the two sidebands and the HFS.

Combining the total systematic uncertainty 493 kHz with the statistic uncertainty 52 kHz, we obtained a total error of 496 kHz. Finally, the HFS was measured at (876.32 ± 0.50) MHz, and the magnetic dipole constant was determined to be A = (219.08 ± 0.12) MHz using equation (4). This is in agreement with previous measurements: (218.9 ± 1.6) MHz [29], (219.3 ± 0.2) MHz [3], (219.12 ± 0.01) MHz [4], (219.125 ± 0.004) MHz [19] and (219.14 ± 0.11) MHz [20], as plotted in figure 6.

5. Conclusion

We have demonstrated a new technique for high-resolution hyperfine splitting measurement of atomic excited states by using the atomic coherence effect of the ladder-type EIT, based on the $6S_{1/2}$–$6P_{1/2}$–$8S_{1/2}$ ladder-type system in the Cs vapour cell around room temperature. Because the EIT spectra have no Doppler background compared with conventional EIT spectra, where the SNR is limited by the absorptive background, the centres of the EIT peaks are well determined by fitting the curves. The frequency axis of the coupling laser is calibrated using a temperature-controlled EOM and a stable confocal F–P cavity to reduce the systematic errors. Given the appropriate length of cavity, and radio frequency driving the EOM, the F–P peaks appear simultaneously with the EIT peaks; hence, error arising from the nonlinear frequency scanning is reduced significantly.

With this kind of frequency calibration method, we are able to measure hyperfine intervals of the $8S_{1/2}$ state for different hyperfine level transitions and obtain an average value of 876.322 MHz with a statistical error of 0.052 MHz. The systematic effects from the ac-Stark and Zeeman shifts were studied. Combining the total systematic uncertainty, 0.495 MHz, with the statistical uncertainty, we obtained a total error of 0.498 MHz. Finally, the hyperfine interval obtained was (876.32 ± 0.50) MHz, and the magnetic dipole constant A = (219.08 ± 0.12) MHz, which is consistent with previous results. This work provides a simple method to measure excited-state hyperfine structure in other atoms that are of interest for parity non-conservation measurements.

Acknowledgments

This work is supported by the National Natural Science Foundation of China (grant nos 61078051, 11104172, 11274213, 61205215 and 61227902), the National Major Scientific Research Program of China (grant no. 2012CB921601), the Project for Excellent Research Team of the National Natural Science Foundation of China (grant no. 61121064), the Shan Xi Scholarship Council of China (grant no. 2012-015) and the Program for Science and Technology Star of Tai Yuan, Shan Xi, People's Republic of China (grant no. 12024707).

References

[1] Wood C S, Bennett S C, Cho D, Masterson B P, Roberts J L, Tanner C E and Wieman C E 1997 Measurement of parity non-conservation and an anapole moment in cesium *Science* **275** 1759–63

[2] Payne M G, Deng L and Thonnard N 1994 Applications of resonance ionization mass spectrometry *Rev. Sci. Instrum.* **65** 2433–59

[3] Herrmann P P, Hoffnagle J, Pedroni A, Schlumpf N and Weis A 1985 Doppler-free spectroscopy of the 8S state of Cs *Opt. Commun.* **56** 22–24

[4] Hagel G, Nesi C, Jozefowski L, Schwob C, Nez F and Biraben F 1999 Accurate measurement of the frequency of the 6S–8S two-photon transitions in cesium *Opt. Commun.* **160** 1–4

[5] Sasada H 1992 Wavelength measurements of the sub-Doppler spectral lines of Rb at 1.3 μm and 1.5 μm *IEEE Photon. Technol. Lett.* **4** 1307–9

[6] Boucher R, Breton M, Cyr N and Têtu M 1992 Dither-free absolute frequency locking of a 1.3 μm DFB laser on ^{87}Rb *IEEE Photon. Technol. Lett.* **4** 327–9

[7] Moon H S, Lee W K, Lee L and Kim J B 2004 Double resonance optical pumping spectrum and its application for frequency stabilization of a laser diode *Appl. Phys. Lett.* **85** 3965–7

[8] Yang B D, Gao J, Zhang T C and Wang J M 2011 Electromagnetically induced transparency without a Doppler background in multilevel ladder-type cesium atomic system *Phys. Rev.* A **83** 013818

[9] Yang B D, Gao J, Liang Q B, Wang J, Zhang T C and Wang J M 2011 Double-resonance optical-pumping effect and ladder-type electromagnetically induced

transparency signal without Doppler background in cesium atomic vapor cell *Chin. Phys.* B **20** 044202
[10] Gao J, Wang J, Yang B D, Zhang T C and Wang J M 2010 Double-resonance optical-pumping spectra of rubidium $5S_{1/2}$–$5P_{3/2}$–$4D_{3/2}$ transitions and frequency stabilization of 1.5 μm laser *Proc. SPIE* **7846** 784618
[11] Menon S and Agarwal G S 2000 Gain components in the Autler–Townes doublet from quantum interferences in decay channels *Phys. Rev.* A **61** 013807
[12] Zibrov A S, Lukin M D, Nikonov D E, Hollberg L, Scully M O, Velichansky V L and Robinson H G 1995 Experimental demonstration of laser oscillation without population inversion via quantum interference in Rb *Phys. Rev. Lett.* **75** 1499–502
[13] Rapol U D, Wasan A and Natarajan V 2003 Subnatural linewidth in room-temperature Rb vapor using a control laser *Phys. Rev.* A **67** 053802
[14] Mohapatra A K, Jackson T R and Adams C S 2007 Coherent optical detection of highly excited Rydberg states using electromagnetically induced transparency *Phys. Rev. Lett.* **98** 113003
[15] Zhao J M, Zhu X B, Zhang L J, Feng Z G, Li C Y and Jia S T 2009 High sensitivity spectroscopy of cesium Rydberg atoms using electromagnetically induced transparency *Opt. Express* **17** 15821–6
[16] Mack M, Karlewski F, Hattermann H, Höckh S, Jessen F, Cano D and Fortágh J 2011 Measurement of absolute transition frequencies of ^{87}Rb to *n*S and *n*D Rydberg states by means of electromagnetically induced transparency *Phys. Rev.* A **83** 052515
[17] Krishna A, Pandey K, Wasan A and Natarajan V 2005 High-resolution hyperfine spectroscopy of excited states using electromagnetically induced transparency *Europhys. Lett.* **72** 221–7
[18] He Z S, Tsai J H, Lee M T, Chang Y Y, Tsai C C and Whang T J 2012 Determination of the cesium 11s $^2S_{1/2}$ hyperfine magnetic coupling constant using electromagnetically induced transparency *J. Phys. Soc. Japan* **81** 124302
[19] Fendel P, Bergeson S D, Udem Th and Hänsch T W 2007 Two-photon frequency comb spectroscopy of the 6S–8S transition in cesium *Opt. Lett.* **32** 701–3
[20] Stalnaker J E, Mbele V, Gerginov V, Fortier T M, Diddams S A, Hollberg L and Tanner C E 2010 Femtosecond frequency comb measurement of absolute frequencies and hyperfine coupling constants in cesium vapor *Phys. Rev.* A **81** 043840
[21] Grove T T, Sanchez-Villicana V, Duncan B C, Maleki S and Gould P L 1995 Two-photon two-color diode laser spectroscopy of the Rb $5D_{5/2}$ state *Phys. Scr.* **52** 271–6
[22] Lee Y C, Chang Y H, Chang Y Y, Chen Y Y, Tsai C C and Chui H C 2011 Hyperfine coupling constants of cesium 7D states using two-photon spectroscopy *Appl. Phys.* A **105** 391–7
[23] Gilbert S L, Watts R N and Wieman C E 1983 Hyperfine-structure measurement of the 7S state of cesium *Phys. Rev.* A **27** 581–2
[24] Yang B D, Gao J, Wang J, Zhang T C and Wang J M 2011 Multiple electromagnetically-induced transparency of hyperfine levels in cesium $6S_{1/2}$ –$6P_{3/2}$ –$8S_{1/2}$ ladder-type system *Acta Phys. Sin.* **60** 114207
[25] Wang J, Wang J M, Liu H F, Yang B D and He J 2013 Measurement of hyperfine splitting and determination of hyperfine structure constant of cesium $8S_{1/2}$ state by using of ladder-type EIT *Proc. SPIE* **8773** 877311
[26] Gea-Banacloche J, Li Y Q, Jin S Z and Xiao M 1995 Electromagnetically induced transparency in ladder-type inhomogeneously broadened media: theory and experiment *Phys. Rev.* A **51** 576–84
[27] Foot C J 2005 *Atomic Physics* (New York: Oxford University Press)
[28] Johnson W R 2007 *Atomic Structure Theory: Lectures on Atomic Physics* (New York: Springer)
[29] Gupta R, Happer W, Lam L K and Svanberg S 1973 Hyperfine-structure measurements of excited S states of the stable isotopes of potassium, rubidium, and cesium by cascade radio-frequency spectroscopy *Phys. Rev.* A **8** 2792–81